

COLLAPSE AND FRAGMENTATION IN FINITE SHEETS

ANDREAS BURKERT¹ AND LEE HARTMANN²

Received 2004 May 26; accepted 2004 July 29

ABSTRACT

We present two-dimensional simulations of finite, self-gravitating gaseous sheets. Unlike the case of infinite sheets, such configurations do not constitute equilibrium states but instead are subject to global collapse unless countered by pressure forces or rotation. The initial effect of finite geometry is to promote concentrations of material at the edges of the sheet. If the sheet is not perfectly circular, gravitational focusing results in enhanced concentrations of mass. In the second-most simple geometry, that of an elliptical outer boundary, the general result is collapse to a filamentary structure with the densest concentrations of mass at the ends of the filament. We suggest that these simple calculations have interesting implications for the gravitational evolution of overall molecular cloud structure, envisioning that such clouds might originate as roughly sheetlike sections of gas accumulated as a result of large-scale flows in the local interstellar medium. We show some examples of local clouds with overall filamentary shape and denser concentrations of mass and star clusters near the ends of the overall extended structure, suggestive of our simple ellipse collapse calculations. We suggest that cluster-forming gas is often concentrated as a result of gravity acting on irregular boundaries; this mechanism can result in very rapid infall of gas, which may be of importance to the formation of massive stars. This picture suggests that much of the supersonic “turbulence” observed in molecular clouds might be gravitationally generated. Our results may provide impetus for further theoretical explorations of global gravitational effects in molecular clouds and their implications for generating the substructure needed for fragmentation into stars and clusters.

Subject headings: ISM: clouds — ISM: structure — stars: formation

1. INTRODUCTION

A central issue in star formation is the origin of the small-scale structure in molecular clouds that leads to the creation of stars. Many researchers have suggested that this substructure is due to “turbulence”; complex, often supersonic, motions lead to density concentrations, which then collapse to form stars (e.g., Larson 1992; Elmegreen 1997; Mac Low et al. 1998; Padoan & Nordlund 1999; Klessen & Burkert 2000, 2001; Ostriker et al. 1999; Klessen et al. 2000; Bate et al. 2002, 2003; Gammie et al. 2003; Li et al. 2004; see also the review by Elmegreen 2002). However, the nature of these supersonic motions is far from clear, making it difficult to evaluate the role of turbulent fragmentation in star formation. For example, small-scale driving of turbulence is employed in many numerical simulations to form stellar mass concentrations, but this may not be consistent with large-scale structure such as the extended massive filaments seen in many clouds (e.g., Schneider & Elmegreen 1979; Hartmann 2002). Another unresolved question is whether the periodic boundary conditions used in many simulations can really capture the essential physics of real clouds, in which material can be either accreted or ejected. More broadly, the recent recognition that molecular clouds have short lifetimes (Elmegreen 2000; Hartmann et al. 2001, hereafter HBB01) emphasizes the likely role of initial conditions in establishing the turbulent velocity field, an area which has not been adequately explored.

A rather different approach to fragmentation was taken by Larson (1985), who pointed out that infinite self-gravitating sheets and filaments have a characteristic scale of fastest

growth, typically a few times the sheet or filament scale height. In this scenario of gravitational fragmentation, gravity acts on a smooth distribution of material in a cloud of limited dimensionality (sheet or filament geometry) but infinite extent to produce fragments of finite mass. This model seems to avoid the need to put smaller (density or velocity) structure in “by hand.” Hartmann (2002) pointed out that the molecular cloud cores in Taurus are elongated in the direction of their host filaments in the sense predicted by gravitational fragmentation. However, the static initial conditions assumed in the simplified Larson (1985) discussion are not consistent with observed supersonic velocity dispersions (e.g., Mizuno et al. 1995). In addition, as we show below, discarding the assumption of infinite sheets or filaments results in crucial modifications to Larson’s picture; finite sheets behave differently.

In this paper we extend the investigations of Larson (1985) to consider structure formation in sheets of finite sizes. We focus on a simplified investigation of initially homogeneous and isothermal sheets to isolate the essential physics of the problem without introducing complications due to heating and cooling processes or turbulent driving. Even within this extremely limited set of conditions, we show that a rich variety of fragmenting structures can arise in gravitationally collapsing finite sheets, including multiple large concentrations that might lead to the formation of clusters and massive stars, with connecting and fragmenting filaments. Our investigations suggest that gravitationally induced motions may be a significant and in many cases dominant contributor to supersonic motions in molecular clouds. We also suggest that boundary effects in general might play an important role; the assumption of periodic boundary conditions in simulations of cloud evolution might therefore neglect important aspects. The importance of boundary effects was first pointed out by Bastien (1983), who studied the collapse of cylindrical clouds. Finally, we also

¹ University Observatory Munich, Scheinerstrasse 1, D-81679 Munich, Germany; burkert@usm.uni-muenchen.de.

² Harvard-Smithsonian Center for Astrophysics, 60 Garden Street, Cambridge, MA 02138; hartmann@cfa.harvard.edu.

speculate on a possible way of relating turbulent structure and initial mass functions.

2. MOTIVATION

HBB01 argued that molecular clouds in the solar neighborhood are mostly formed as a result of large-scale flows, which pile up atomic gas until sufficient column densities are accumulated to shield the gas from the interstellar ultraviolet radiation field and allow molecules to form. The flows are presumed to be driven by stellar energy input, principally supernovae. The resulting clouds are then formed as wall sections of “bubbles” (e.g., Vazquez-Semadeni et al. 1995; Passot et al. 1995; de Avillez & Mac Low 2001; Wada & Norman 2001; HBB01 and references therein).

The simplest abstraction of this picture of cloud formation (which is also consistent with cloud formation behind a shock front, such as in a spiral density wave) is a flat uniform sheet of finite dimensions. While real clouds formed by flows obviously will not be perfectly flat or have uniform surface densities initially, it seems appropriate to make an initial exploration to isolate the effects of gravity on sheets with finite structure. To further simplify the analysis we assume isothermality and consider sheets that either are static or have simple, smooth velocity fields. Even with these restrictive assumptions, a wide variety of behavior results, which may have more general implications.

Before presenting the simulations, it is instructive to start by considering some analytic results and approximations that illustrate some basic properties. We start with the simple case of a static, isothermal, infinite, infinitely thin sheet with an initially constant surface mass density Σ_0 . In this case the dispersion relation is (Larson 1985)

$$\Gamma^2 = 2\pi G\Sigma_0 k - c_s^2 k^2, \quad (1)$$

where Γ is the exponential growth rate. There is a critical wavenumber,

$$k_c = 2\pi G\Sigma_0/c_s^2, \quad (2)$$

above which no exponential growth is possible; i.e., there is a minimum wavelength (a Jeans length) for gravitational instability. Differentiating equation (1) with respect to k , one can find the wavenumber at which the exponential growth is fastest,

$$k_f = \pi G\Sigma_0/c_s^2 = k_c/2. \quad (3)$$

This result suggests that the sheet will break up into fragments of preferred mass

$$M_f \sim \lambda_f^2 \Sigma = 4c_s^4/(G^2 \Sigma_0), \quad (4)$$

where $\lambda_f = 2\pi/k_f$. Similar results hold for a self-gravitating sheet of finite thickness in hydrostatic equilibrium with the critical wavenumber reduced by a factor of 2. Fragmentation of an infinite filament similarly occurs on some small multiple of the thickness of the configuration (Larson 1985).

As pointed out by Larson (1985), although there is a critical wavelength for gravitational collapse in a uniform density medium (the Jeans length), it is difficult to fragment in such a situation, for instance in a uniform density sphere, because the

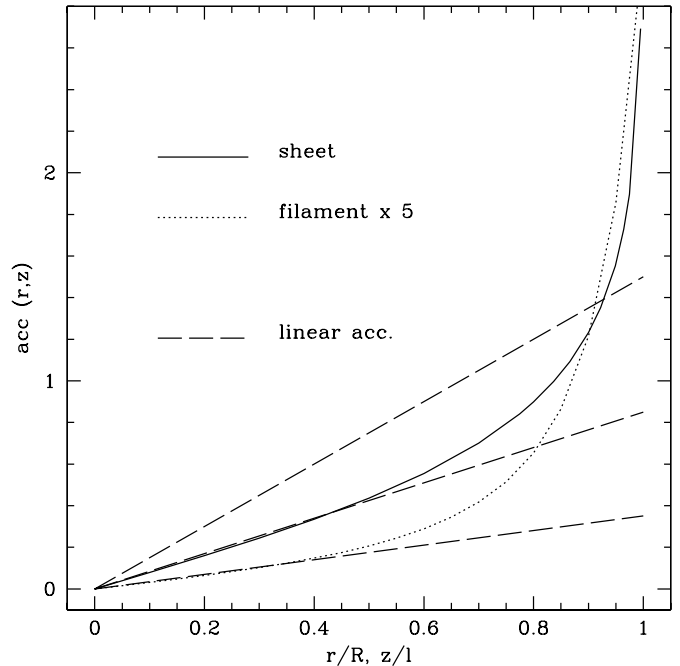


FIG. 1.—Gravitational acceleration for the uniform sheet (eq. [6]; *solid line*) in units of $4G\Sigma$ vs. radial distance in units of total sheet radius r/R , along with the acceleration for the uniform filament (eq. [10]; *dotted line*) in units of $G\rho/5$. Various linear terms are indicated by dashed lines (see text).

growth rate increases monotonically with increasing wavelength (decreasing wavenumber); large-scale collapse tends to overwhelm fragments (Tohline 1980). In contrast to the uniform sphere case, infinite sheet or filament models do exhibit a characteristic scale of growth. However, these initial equilibrium states require an infinite extent of the sheet or filament, and real clouds cannot be infinite. This leads to some important changes in the sheet/filament picture of fragmentation.

The gravitational potential at a point r from the center of an infinitely thin, uniform surface density sheet of radius R is (Wyse & Mayall 1942)

$$\Phi = -4G\Sigma RE(r/R), \quad (5)$$

where Σ is the surface density and E is the second complete elliptic integral. The gravitational acceleration toward the center at r is

$$a_r = -\frac{\partial\Phi}{\partial r} = 4G\Sigma \frac{R}{r} \left[K\left(\frac{r}{R}\right) - E\left(\frac{r}{R}\right) \right], \quad (6)$$

where K is the first complete elliptic integral. The acceleration goes to infinity at $d = R$, which would not occur in a sheet with finite thickness; thus, we restrict use of this equation to regions considerably more than a sheet thickness from the edge.

Figure 1 shows the acceleration in units of $4G\Sigma$ as a function of r/R . The steep increase of inward acceleration as $r \rightarrow R$ implies that the sheet, initially at rest, will immediately proceed to collapse, with material piling up most rapidly at the outer edge (limited by gas pressure gradients, which we ignore here, i.e., we are assuming that the sheet contains many Jeans masses).

It is useful to estimate the timescale of global collapse for comparison with numerical results. Using the expansions of

the K and E integrals (Abramowitz & Stegun 1972), equation (6) can be written as

$$a_r = \frac{1}{2} \frac{dv^2}{dr} = \pi G \Sigma \left[\frac{r}{R} + \frac{3}{8} \left(\frac{r}{R} \right)^3 + \frac{45}{192} \left(\frac{r}{R} \right)^5 + \dots \right]. \quad (7)$$

Ignoring pressure support, a collapse timescale t_c can be estimated for a subregion of size δv lying in the inner region of the sheet of radius R . Integrating equation (7) using only the linear term, starting from rest, and assuming that Σ does not change significantly within the inner region (see § 3.1), a typical infall velocity of the subregion is

$$v^2 = \frac{\pi G \Sigma}{R} (\delta r)^2, \quad (8)$$

and thus

$$t_c = \frac{\delta r}{v} = \left(\frac{R}{\pi G \Sigma} \right)^{1/2}. \quad (9)$$

Note that t_c is independent of the size of the region δr , a result that is used in § 3.1. While this collapse timescale ignores the nonlinear acceleration and thus does not describe the pile-up of material at the edge, we find numerically that t_c is a good estimate of the time it takes for the edge of the circular sheet to fall to the center (§ 3.1).

Without rotation or some other motion, the ultimate fate of this circular sheet is to collapse entirely to the center. The dashed lines in Figure 1 show linear forms for a_r ; the middle dashed line indicates the situation in which an outward acceleration is comparable to the first term in the expansion of equation (7), which balances the inward gravitational acceleration of the inner region. Solid-body rotation, with centripetal acceleration $a(c)_r = -\Omega^2 r \propto r$, where Ω is a constant, could in principle be such an example, preventing collapse in the inner sheet regions. However, the nonlinear acceleration as $r \rightarrow R$ shows that such rotation cannot stop the edge from collapsing to a ring whose dimensions are set by angular momentum. Moreover, the uniformly rotating sheet, whether in the non-equilibrium case of constant surface density or in the equilibrium case of $\Sigma \propto [1 - (r/R)^2]^{1/2}$ (Mestel 1963), is unstable to large-scale perturbations (Hunter 1963) and generally results in large-scale redistribution of material with a concentration of mass to the center (see, e.g., Binney & Tremaine 1987, pp. 374–375). Conversely, large rotation (such as indicated by the upper dashed curve) could prevent the inner region from collapsing but only at the expense of having the interior expand and the edge collapse to an outer ring.

The finite filament exhibits similar behavior. For a uniform cylindrical filament of radius h and length $2l$, the acceleration toward the center at a point on the axis lying a distance z from the center is

$$a_z = -2\pi G \rho \left\{ 2z - [h^2 + (l+z)^2]^{1/2} + [h^2 + (l-z)^2]^{1/2} \right\}, \quad (10)$$

where ρ is the density of the filament. When $l \gg h$ and when considering points away from the exact end of the filament, $l-z \gg h$,

$$a_z \approx -\pi G \rho h^2 [(l+z)^{-1} + (l-z)^{-1}]. \quad (11)$$

However, $\pi \rho h^2 = m$, the mass per unit length of the filament. Using this relation and expanding the quantity in brackets, we have

$$a_z \approx -Gm \left(\frac{2z}{l^2 - z^2} \right). \quad (12)$$

Figure 1 also shows the acceleration of a thin filament in units of $G\rho$. Note that the acceleration of an infinitely thin filament goes to infinity at its edge (eq. [11]), just as in the case of the infinitely thin sheet, but this singularity disappears for finite h (eq. [10]).

As in the case of the sheet, solid-body rotation of the filament (*lower dashed curve*) can help stabilize the collapse of the inner regions but cannot prevent the ends of the filament from collapsing initially. Alternatively, if one wants to prevent the filament ends from collapsing, the solid-body rotation would force the inner regions to expand away toward the ends of the filament, resulting in concentrations at the endpoints.

These simple considerations illustrate the universal tendency for material to pile up and concentrate at edges of finite structures because of gravity. Whether the local sheet fragmentation can take place as envisaged by Larson (1985) depends upon whether the *global* collapse overtakes or prevents *local* collapse. This is investigated numerically in § 3.

3. NUMERICAL SIMULATIONS

The numerical calculations are performed on a two-dimensional Eulerian, Cartesian grid. The full computational region with dimension $2 \times L$ is represented by a grid composed of $N \times N$ grid cells equally spaced in both directions. Under the assumption of isothermality, the relevant differential equations to be integrated are the hydrodynamic continuity and momentum equations:

$$\begin{aligned} \frac{\partial \Sigma}{\partial t} + \nabla \cdot (\Sigma \mathbf{v}) &= 0 \\ \frac{\partial \mathbf{v}}{\partial t} + (\mathbf{v} \cdot \nabla) \mathbf{v} &= -\frac{\nabla P}{\Sigma} - \nabla \Phi, \end{aligned} \quad (13)$$

where $\Sigma(\mathbf{x})$, $P(\mathbf{x})$, and $\mathbf{v}(\mathbf{x})$ are the gas surface density, pressure, and two-dimensional velocity vector at position \mathbf{x} , respectively. The gravitational potential Φ is determined by solving Poisson's equation in the equatorial plane (Binney & Tremaine 1987),

$$\nabla^2 \Phi = 4\pi G \Sigma, \quad (14)$$

where G is the gravitational constant. The isothermal equation of state

$$P = c_s^2 \Sigma \quad (15)$$

determines the pressure for a given surface density Σ and sound speed c_s .

This set of equations is integrated numerically by means of an explicit finite second-order van Leer difference scheme including operator splitting and monotonic transport as tested and described in detail in Burkert & Bodenheimer (1993, 1996). In order to suppress numerical instabilities, an artificial viscosity of the type described by Colella & Woodward (1984) is added (Burkert et al. 1997).

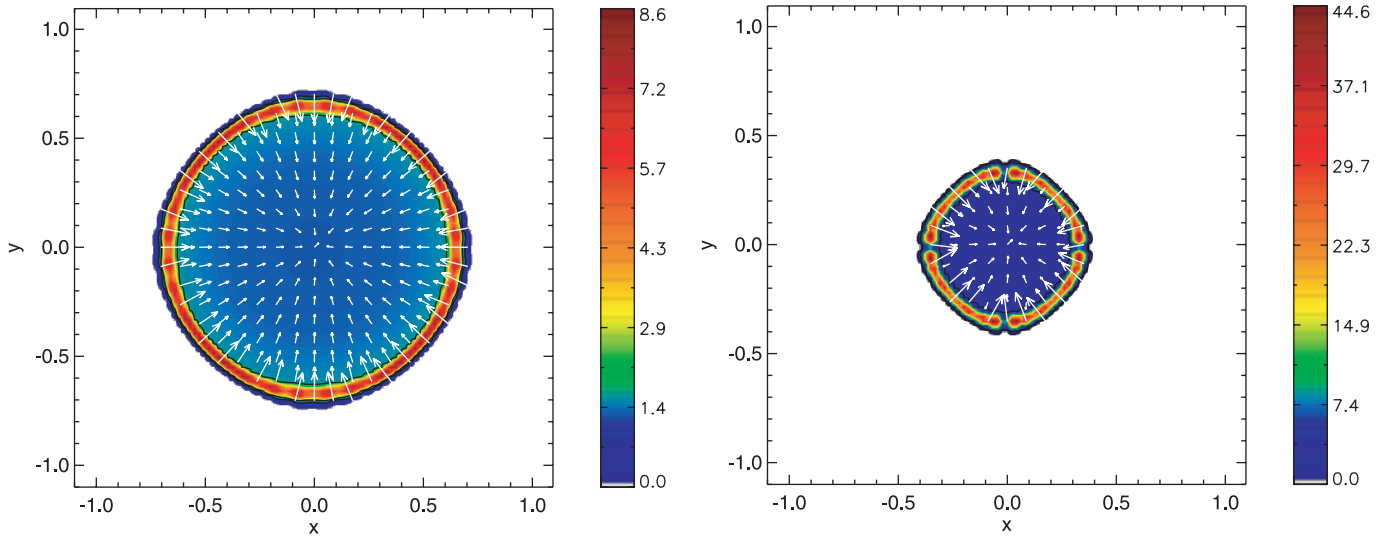


FIG. 2.—Numerical simulation of the collapse of the finite two-dimensional sheet. In this calculation the initial sheet surface density is set to unity, $G = 1$, and the sound speed is 0.1 in appropriate units (see text). In code units, the time at which the snapshot is taken in the left panel is 0.285; for the right panel $t = 0.429$. The gaps in the outer ring on the x -axis and y -axis in the left panel are purely numerical and caused by the representation of the circular sheet by a Cartesian grid.

The Poisson equation is integrated on the grid under the assumption that there is no matter outside of the computational region. As we are focusing here on the gravitationally unstable sheets that collapse toward the center of the region, outflow of gas beyond the outer boundaries can be neglected. Therefore, the outflow velocities at the outer boundary are set to zero and a negligible pressure gradient is assumed. Most calculations were typically performed with 100^2 grid cells of size $\Delta = 2L/N$ and height Δ , where $2L$ is the largest dimension of the rectangular computational region. Test calculations with $N = 200$ and 500 did not result in significant differences. In these calculations the code units were set such that $G = 1$.

3.1. Static Circular Sheet

Figure 2 shows the evolution of a static sheet with initially uniform surface density (in code units, $\Sigma = 1$), of circular shape, $R = 1$, and with sound speed $c_s = 0.1$ (inside a computational region of $L = 1.1$). The mass of this sheet is thus $\pi\Sigma R^2 = \pi$ in code units. Larson (1985) notes that the Jeans mass for circular modes in an infinite thin static sheet is

$$M_c = 1.17c_s^4/(G^2\Sigma); \quad (16)$$

thus, this sheet initially contains $\sim 10^4$ Jeans masses. As expected, material initially piles up at the edge (*left*). Note that even at an early stage, collapse in the inner regions is noticeable. The evolution of the sheet is simple; the edge grows as it falls in, and the entire structure collapses (*right*).

We never found any evidence for gravitational growth of fragments in the inner region, even for $c_s = 0$. Some fragmentation is seen in the piled-up ring material, which is due to the growth of initial numerical noise, especially on the x - and y -axes, much of which is generated by the initial structure of a circular edge approximated in a rectangular grid. More and earlier fragmentation in the ring occurs as the sound speed is decreased. The details of fragmentation in this and the further simulations to be discussed should not be believed, as resolution quickly becomes an issue; here we are concentrating on global structure.

We ran a number of simulations for differing values of the sound speed; as long as the initial sheet contained many Jeans masses, i.e., the sheet was sufficiently cold, the results were similar. For warm sheets of a few Jeans masses, fragmentation due to numerical fluctuations in the edge ring was suppressed. Finally, if the mass of the sheet was small, the sheet “bounced” and then eventually adjusted to a static equilibrium.

Figure 3 shows the density and velocity structure of the simulation shown in Figure 2. Note the pile-up of material and also that infall develops rapidly in the inner regions as well, as expected from the analytic results of § 2. The collapse timescale in the linear (inner sheet) regime, equation (9), is $\pi^{-1/2} = 0.564$ in code units. For the particular case described above, the time taken for the edge to reach the center is approximately $t_g \sim 0.51$, i.e., slightly shorter than the linear timescale.

The above result for the timescale of global versus local collapse helps to explain why we never found any indication of small-scale, linear perturbations becoming large before the entire sheet collapsed. The infall, which develops rapidly in all sheet regions, apparently invalidates the linear analysis of the infinite, static sheet. Consider the following argument: The most favorable location for a finite perturbation (larger than a Jeans length) to grow before being overtaken by the general collapse is at the center of the sheet, where the edge material takes the longest time to arrive. We may use the result of equation (9) to evaluate the timescale of local collapse in the limit of zero sound speed (negligible gas pressure), because this term simply represents gravitational acceleration. Moreover, as shown in Figure 3, even during the collapse the surface density tends to remain uniform and the velocity gradient similar until the infalling “edge” material overtakes it. Now, equation (9) indicates that the timescale for collapse is *independent* of the radius of the perturbed region; moreover, we find numerically that the time for the edge material to reach the origin is slightly less than this value. Thus, small perturbations cannot amplify before being swept up by the overall collapse. Because the collapse time in equation (9) is proportional to $\Sigma^{-1/2}$, only very nonlinear perturbations have a chance to grow before being swallowed up by the global collapse. The situation is analogous to the collapse of a uniform sphere, for which all radii reach the

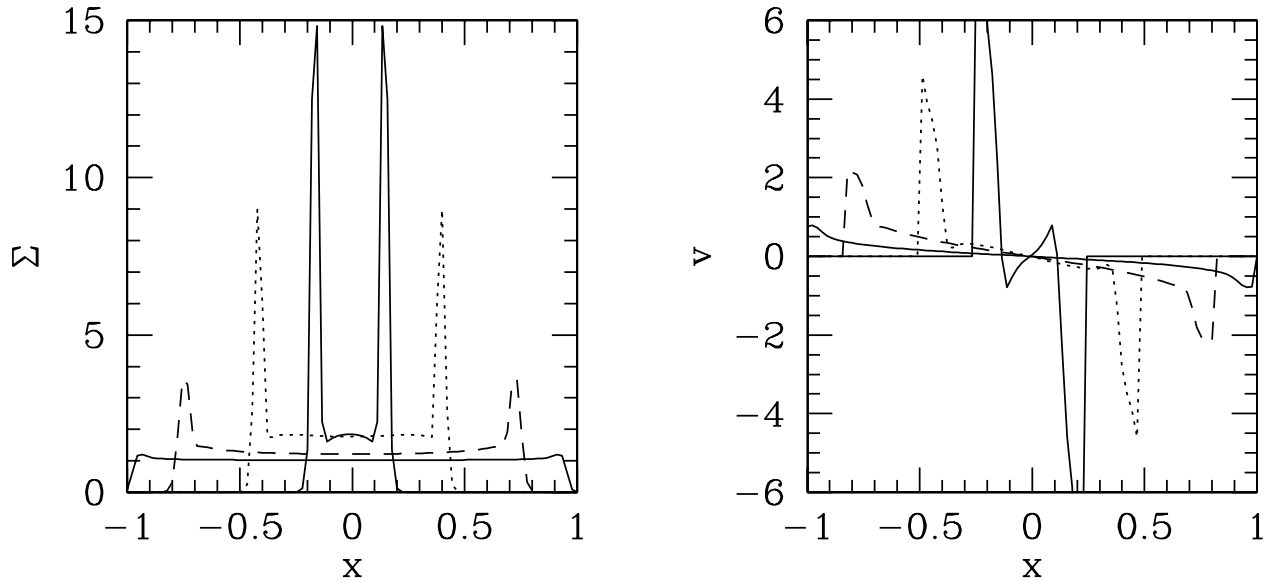


FIG. 3.—Evolution of the density and velocity of the circular sheet collapse of Fig. 2. The snapshots are taken at times $t = 0.09, 0.25, 0.41,$ and 0.49 (outer solid, dashed, dotted, and inner solid curves, respectively). Note the flat density distribution and the linear velocity gradient in the inner regions, as expected from the result in eq. (8), until late in the evolution, when inner material begins to fall outward because of the gravity of the infalling edge.

center at the same time, preventing effective fragmentation from small perturbations (Larson 1985).

Even fairly large perturbations have difficulty growing before overall collapse of the edge wins. This is shown in Figure 4, in which we show the evolution of an initial 10% ringlike perturbation as a function of time. The surface density of the perturbation grows linearly with time but never outruns the edge, the latter eventually overtaking it.

3.2. Static Ellipse

Figure 5 shows the evolution of an elliptical sheet with an initial ellipticity of $e = 0.6$. Again we assume $c_s = 0.1$. As in the case of the circular sheet, material piles up at the edge as the entire configuration collapses. However, a new feature arises: specifically, “focal points” appear where gravity acts on the

curvature of the sheet edge to produce large, dense mass concentrations close to or outside of the foci of the initial elliptical structure (*top right*). These mass concentrations grow with respect to the rest of the edge material by gravitationally attracting neighboring material to fall into them (*bottom left*). Finally, the sheet collapses into a filamentary structure with large mass concentrations at both ends.

The geometry leading to focal points is indicated schematically in Figure 6. Any sheet edge that locally has a smaller radius of curvature than the larger-scale sheet geometry will yield a local focus for gravitationally collapsing material.

As before, our limited resolution prohibits any quantitative analysis of the number, masses, and sizes of fragments that eventually condense along the filament. The inhomogeneities present along the filament are the result of numerical noise and

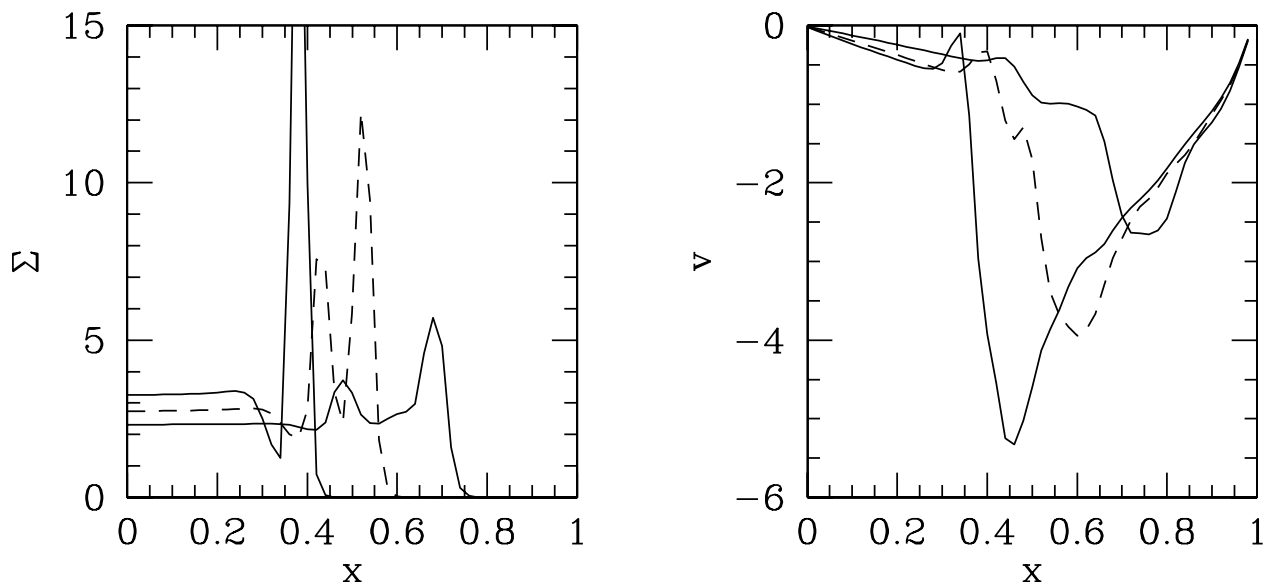


FIG. 4.—Evolution of the uniform circular sheet with a ringlike perturbation of excess surface density at times $t = 0.15, 0.21,$ and 0.26 (outer solid, dashed, and inner solid curves, respectively). The perturbation grows as the sheet collapses, but not nonlinearly, and is eventually overtaken by the collapse of the edge (see text).

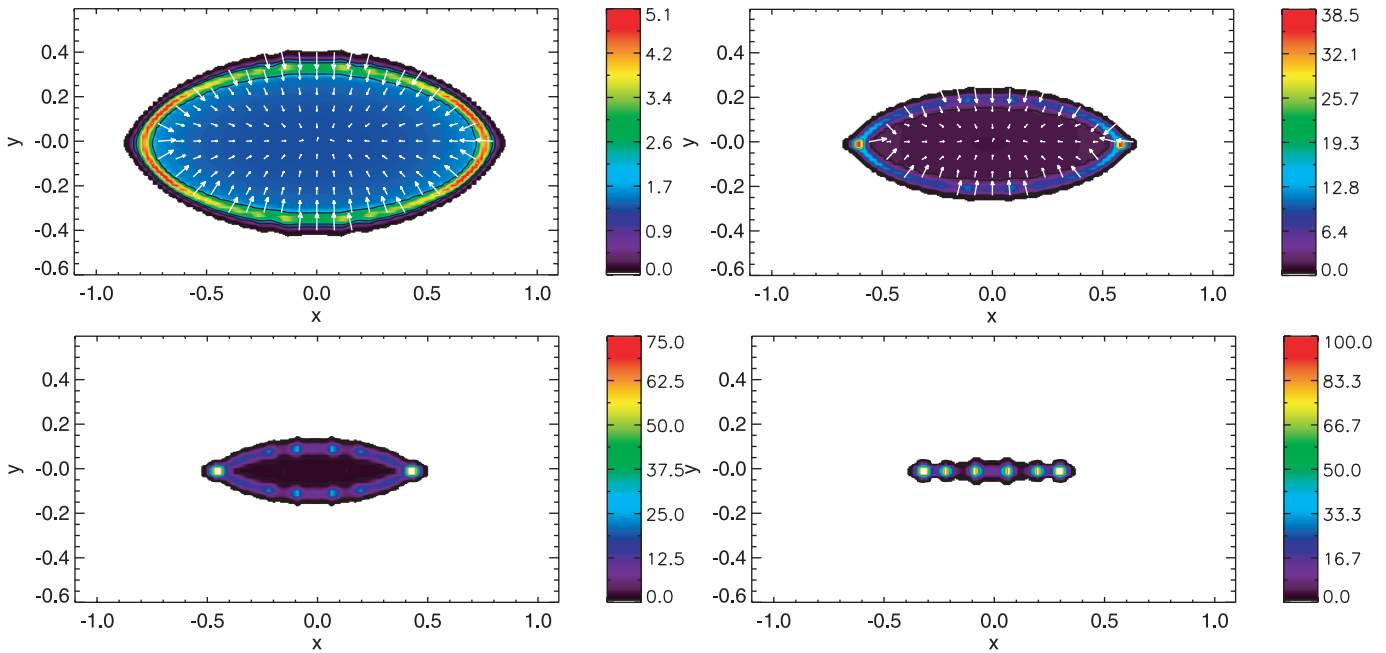


FIG. 5.—Collapse of a static elliptical sheet. *Top left:* At $t = 0.23$. Material piles up at the edge as the sheet collapses. *Top right:* At $t = 0.33$. Material accumulates particularly at focal points at the ends of the ellipse. *Bottom left:* At $t = 0.39$. Focal points become more prominent. *Bottom right:* At $t = 0.44$. Collapse to a filament has occurred, with major concentrations at the ends.

limited resolution (e.g., Truelove et al. 1997), which get amplified during collapse. Our main points are simply that the elongated sheet tends to collapse to a filament and that focal points develop, which results in larger concentrations of mass at the filament ends, a result seen, for example, in simulations of the collapse of elongated gas clouds (Bastien 1983; Bonnell et al. 1991; Burkert & Bodenheimer 1993).

3.3. Sheets without Sharp Edges

The previous calculations assumed a sharp outer edge, where the surface density decreases by 2 orders of magnitude.

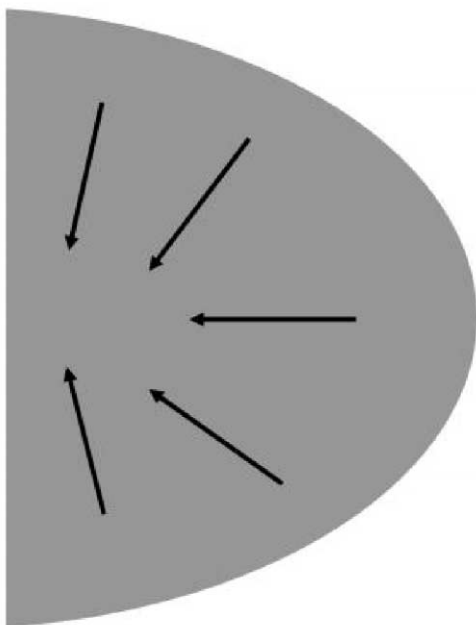


FIG. 6.—Schematic geometry leading to mass concentration at a “focal point” (see text).

It seems implausible that real sheetlike clouds should have such sharp edges, so we investigate a case in which the transition at the cloud boundary is more gradual. Figure 7 shows what happens when the density distribution of the elliptical sheet falls off toward the edge. In this particular case the density is made to fall off smoothly to zero starting at 80% of the distance to the elliptical boundary. As shown in Figure 7 (*left*), an edge concentration still develops but in a smaller structure; there is a modest amount of material outside this edge. Focal points develop as before. Finally, as shown in Figure 7 (*right*), collapse to a filament once again occurs, with mass concentrations near the end, but now lower density material extends outside of the focal point concentrations. Note that Nelson & Papaloizou (1993) found that spheroids did not necessarily form concentrations at each end if the density distribution tapered off sufficiently. Uniform-density spheroids tend to have larger masses per unit lengths at their centers than the corresponding uniform sheets, suggesting that the difference between two and three dimensions can be important.

3.4. Expanding Sheets

If sheets are made as parts of the walls of “bubbles” driven by supernova explosions or stellar winds, they will generally exhibit some expansion in the direction perpendicular to the main flow. In our two-dimensional approximation, ignoring the bubble wall curvature, we can introduce a similar effect by putting in a linear expansion term. Figure 8 shows an expanding case, which was designed such that gravity was not strong enough to reverse the expansion in the inner region but was still large enough to play a role at the outer edge. The initial radial velocity was assumed to increase linearly with distance from the center, and the surface density was constant. Note that the entire region expands, but there is still a pile-up of material at the edge and the formation of focal points. Thus, expansion does not qualitatively change the mass concentration, although it prevents the overall collapse of the sheet.

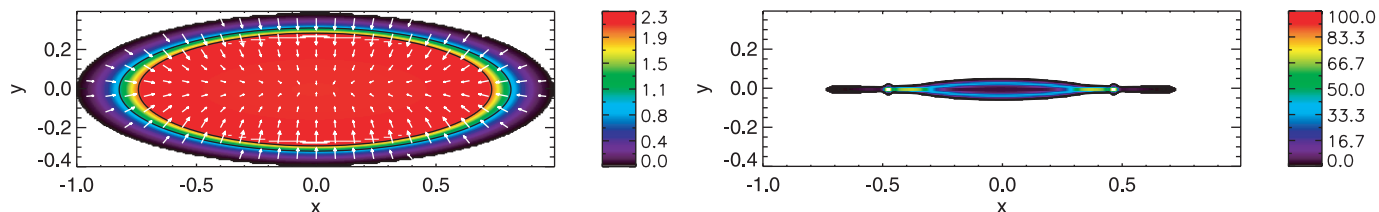


FIG. 7.—Evolution of the static elliptical sheet with density decreasing to the edge. The main features of the uniform ellipse are retained: a pile-up of material still occurs (although on a smaller scale), more material lags outside the edge (*left*), and the final filament formed shows mass concentrations somewhat interior to the ends of the filamentary gas (*right*) (see text).

3.5. Rotating Sheets

In general, there can be some angular momentum present in the plane of the sheet. Figure 9 shows the case of a uniformly rotating elliptical sheet. Again, focal points form and collapse to a filament, with larger mass concentrations at the ends of the filament (see also earlier work by Bonnell et al. 1991; Nelson & Papaloizou 1993; Monaghan 1994). The rotation of the resulting filament (Fig. 10, *left*) is sufficient to slow the overall collapse. Material along the filament starts to be pulled in by the focal-point concentrations near the ends of the filament.

We again emphasize that the number and properties of fragments in the filament are not quantitatively reliable. (Note that fragmentation of rotating filaments has also been found, e.g., by Monaghan 1994.) Nevertheless, as a qualitative result it is interesting to inquire what velocity structure would be seen by an observer in the plane of the sheet (now the plane of the filament). Figure 10 (*right*) shows a contour plot of surface density integrated along the y -direction as a function of the velocity in the x -direction, when the two edges have merged into the connecting filament. In addition to the evident overall rotation, there are local velocity perturbations due to the gravitational accelerations of the various mass concentrations (an effect earlier seen in the simulations of fragmenting cylindrical clouds by Bonnell & Bastien 1993; e.g., their Figs. 3–5). The original total mass of the ellipse was 1.26 in code units, and the initial major axis was unity, so one would expect gravitationally induced velocities to be of order $v_{\text{dyn}} \sim (GM/R)^{1/2} \approx$ unity; the overall velocity gradient in the line of sight is in agreement with this estimate. The “turbulence” in the line of sight, i.e., local fluctuations due to gravitational perturbations by local concentrations, is also of this order. The qualitative idea that differing mass concentrations along a filament can (and must) induce smaller scale velocity structure (“turbulence”) is worth noting. Our results bear an interesting qualitative resemblance to the velocity gradients seen in the ^{13}CO emission of the Orion A cloud (Bally et al. 1987; see § 4.2).

3.6. Ellipse with Surface Density Gradient

It would be surprising if sheetlike clouds in the interstellar medium were uniform in surface density. We consider the next most complicated case, that of a uniform linear surface density gradient along the major axis of the elliptical sheet. Figure 11 shows what happens in the case in which the surface density varies by a factor of 4 from one end of the ellipse to the other, with $\Sigma = 2$ at the right end and $\Sigma = 0.5$ at the left. The evolution is basically the same as that of the uniform ellipse, except that the dense edge and focal point develop only at the dense end.

3.7. “Ghosts”

It would be surprising if real clouds had perfectly smooth boundaries of either circular or elliptical shape. As indicated schematically in Figure 6, any irregularity with a small radius of curvature will tend to produce a concentration. To explore the qualitative nature of a complex boundary, in Figure 12 we show the results of the collapse of a sheet with uniform initial surface density but an arbitrary irregular boundary (the “ghost”). As shown in the sequence of figures, pile-up of material occurs first along the edge, as before; focal points develop soon after. As collapse proceeds, more material is pulled into the focal concentrations, which fall in toward the origin. Near the end of the calculation, most of the mass lies in concentrations, in numbers initially reflecting the number of initial “nodes” in the original boundary; merging and subsequent evolution probably occurs, but we cannot follow it in detail with our resolution.

4. DISCUSSION

4.1. Initial Conditions

Our results show the powerful tendency of finite self-gravitating sheets to develop structure as a result of gravitational focusing. This immediately raises the question: how relevant are these highly simplified calculations? Real clouds are likely to have much more initial structure than what we have imposed in our simulations; however, this should simply

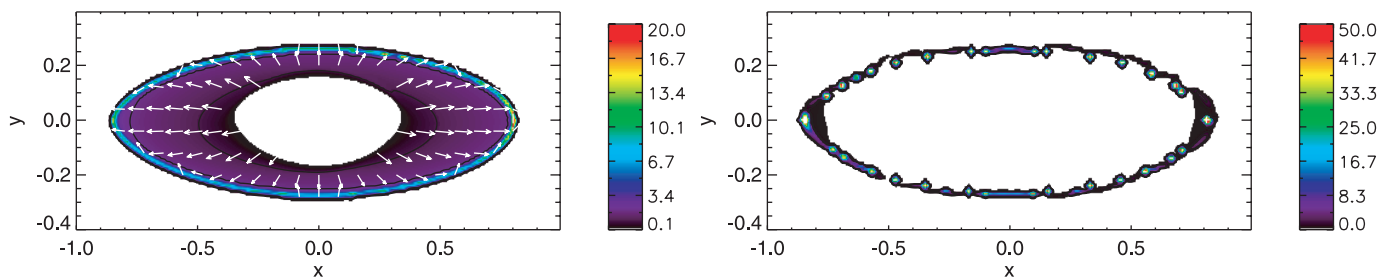


FIG. 8.—Results for an expanding elliptical sheet. Material moves outward from the origin to add to the edge, which still forms a concentration (*left*). Ultimately, most of the mass ends up in the expanding edge, with fragments determined by numerical noise and resolution (*right*) (see text).

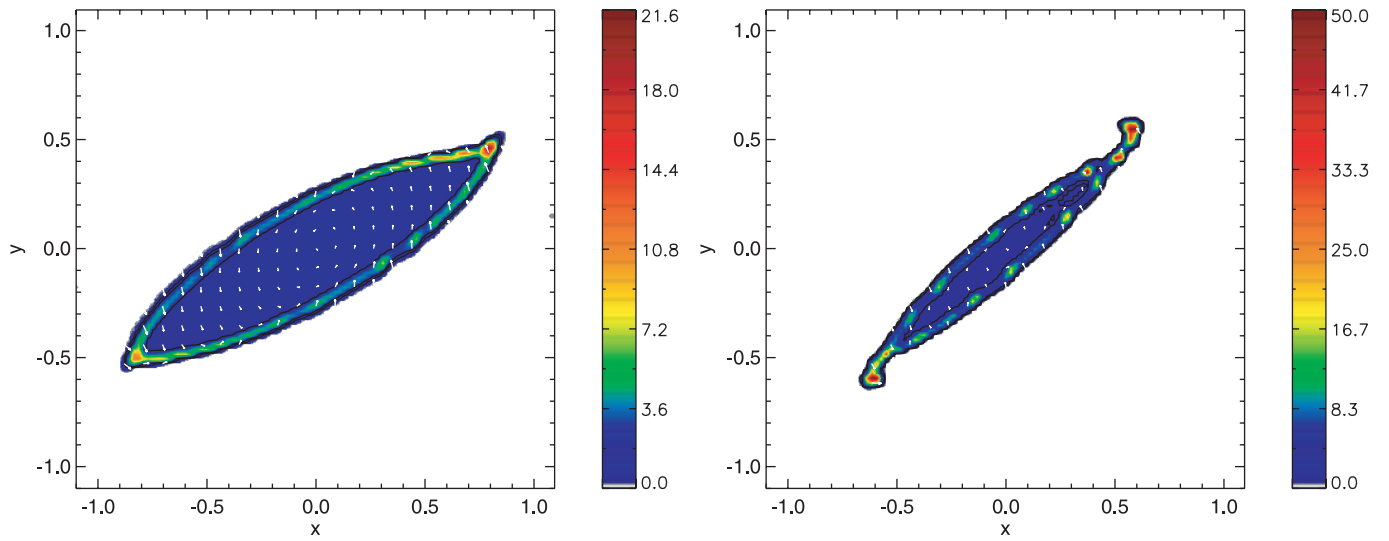


FIG. 9.—Collapse of the rigidly rotating elliptical uniform sheet. Focal points form, and an eventual filament results (see also Fig. 10) that has significant rotational support against gravity (see text).

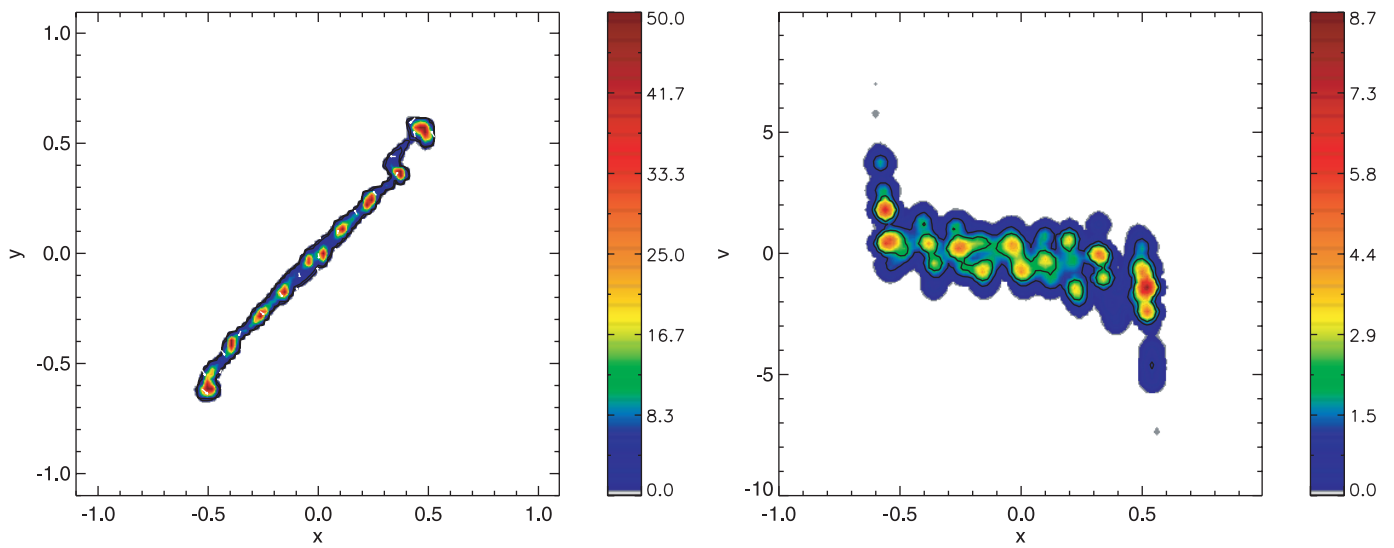


FIG. 10.—*Left*: Formation of a filament from the rotating ellipse simulation (Fig. 9). The size and number of subfragments are not quantitatively reliable. *Right*: Contours of constant surface density integrated in the y -direction as a function of velocity in the x -direction (see text).

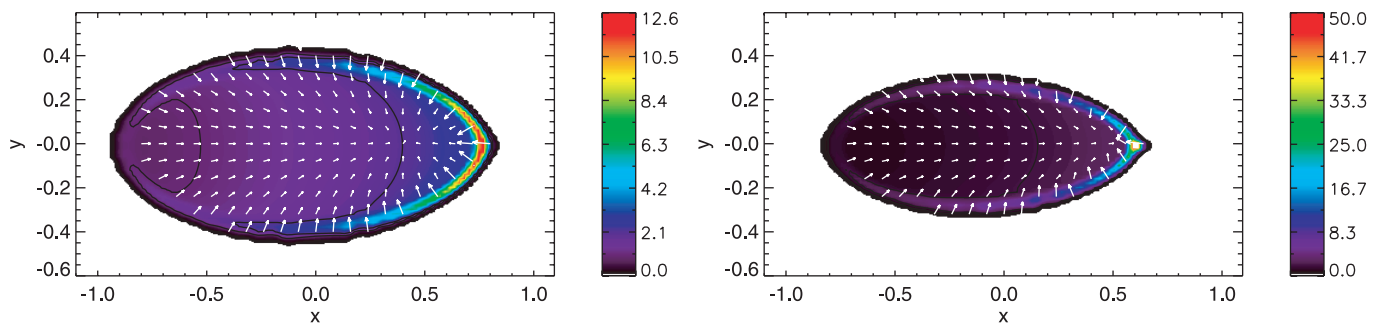


FIG. 11.—Evolution of the static elliptical sheet with a linear surface density gradient along the major axis. The resulting evolution is similar to the uniform ellipse, except that the dense edge and focal point concentration develop only at one end (see text).

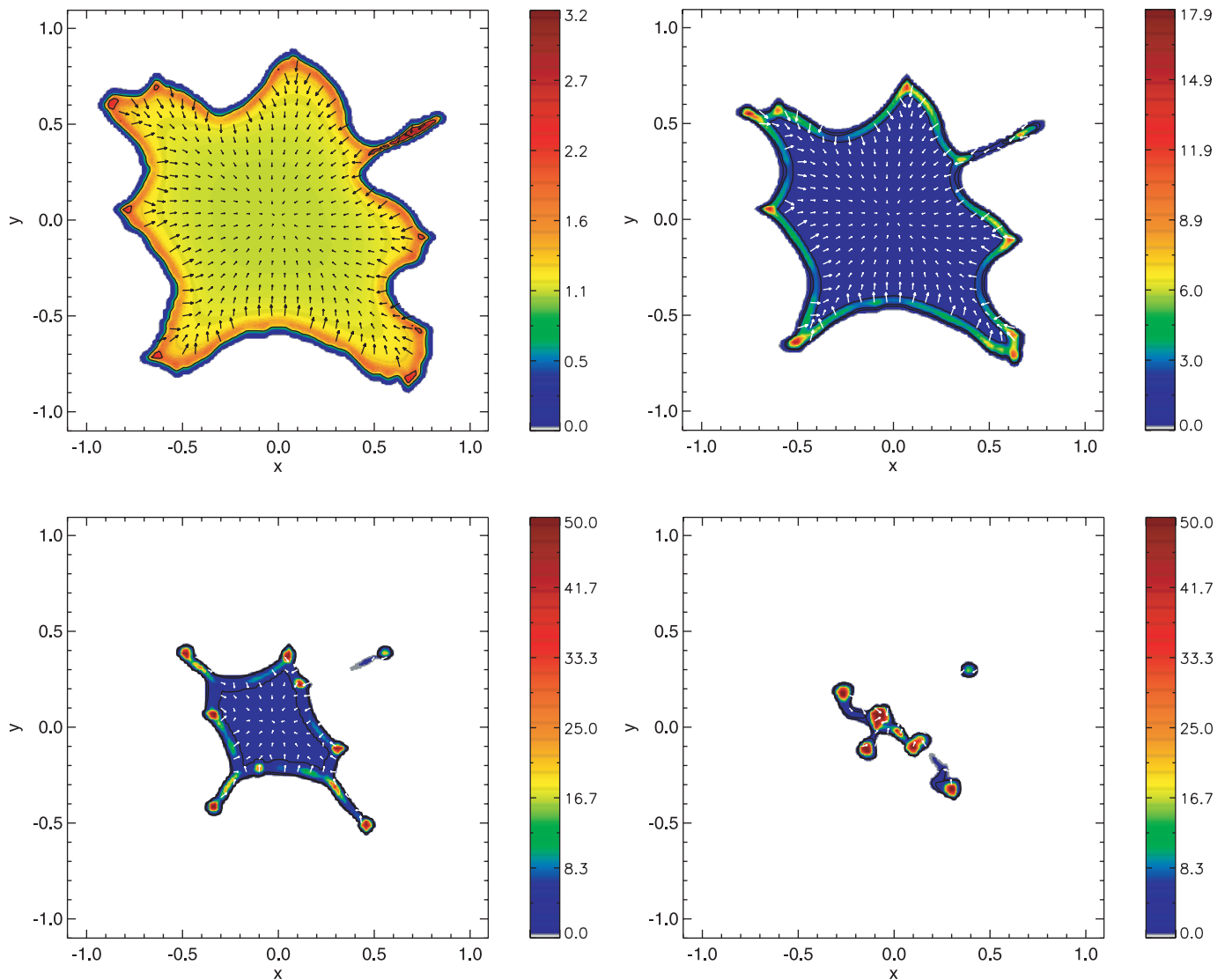


FIG. 12.—Collapse of the “ghost,” a sheet with a highly irregular boundary (see text).

generate more substructure due to local focusing effects. Similarly, the overall tendency for a noncircular sheet to collapse to a filament should also be robust; more initial substructure will not stop the global collapse to a filament, although the detailed structure could be much more complex.

Because a finite self-gravitating sheet will immediately start to collapse at its edges, our assumption of static initial edge structure is probably not very realistic. However, we think that this complication does not matter very much. As real molecular clouds are accumulated out of material in the diffuse interstellar medium, collapse will start, leading to concentrations at edges some time before the final cloud mass has been accreted; but because this process is so rapid, it is not important whether or not this is regarded as an initial condition or as an early development. Perhaps our results for the sheet with a decline in density near the outer edge (Fig. 11) can be thought of as indicating the evolution in a case in which material is still being accumulated in outer regions as the interior collapses. As discussed in the previous sections, such edge effects can only be avoided by using substantial differential rotation or internal pressure gradients in ways that are not clearly relevant to most molecular clouds.

Of course, the formation of real clouds by flows will introduce some density inhomogeneities and velocity perturbations. Thus, one can expect the structure of real clouds to develop in a much more complex way than considered here. But we suggest, as demonstrated in § 4.2, that our results may be relevant to the large-scale or overall morphology of at least some molecular clouds, with significant substructure superimposed by velocity and density perturbations.

Broadly speaking, our results are a simple case of the more general proposition of Ballesteros-Paredes et al. (1999) that molecular clouds cannot be in virial equilibrium. As a technical matter, our calculations also suggest that the occasional practice in numerical simulations of “turning on” gravity after some evolution is not appropriate; gravity has long-range effects that must be considered. In addition, it seems clear that computational boxes with periodic boundary conditions will not capture potentially important evolution.

4.2. Cloud Morphologies

It is obvious that a huge variety of shapes and fragments can result from sufficiently complicated initial conditions at sheet edges or from a spectrum of density fluctuations within sheets.

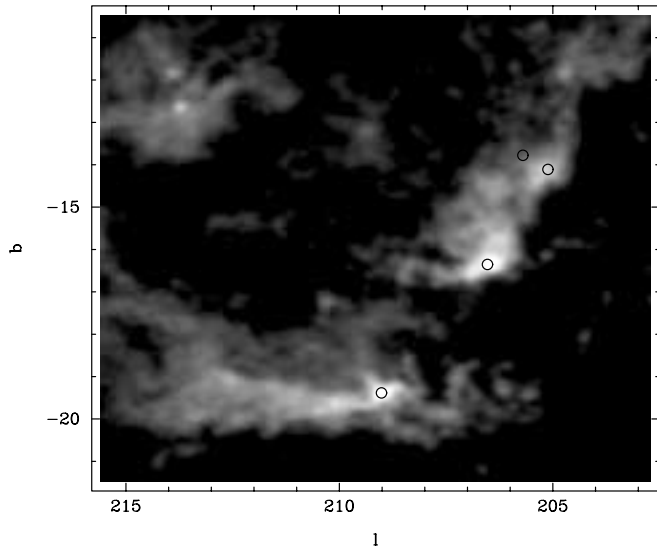


FIG. 13.—Large-scale distribution of integrated ^{12}CO emission in the region of Orion shown as a function of Galactic longitude and latitude (from Wilson 2001). Positions of the Orion Nebula cluster and the young NGC 2024, 2068, and 2071 clusters are marked by superposed circles (see text).

Taking the larger view, it is interesting to note that already the second-simplest figure, an elliptical sheet, produces filaments with larger mass concentrations at each end. This result suggests that clouds initially are likely to be noncircular even if sheetlike configurations of this type might be fairly common. Here we briefly consider the morphology of some well-known local star-forming regions in light of our simplified collapse calculations.

Figure 13 shows the large-scale distribution of ^{12}CO emission in the Orion A and B clouds (Wilson 2001). The overall morphology of the clouds suggests part of an arc, such as might be produced by an expanding, flow-driven bubble that accumulates material far out of the Galactic plane (HBB01). The overall structure is highly filamentary, especially in the A cloud. Strikingly, the massive Orion Nebula cluster (Hillenbrand 1997 and references therein) and the young, dense embedded clusters NGC 2024, 2068, and 2071 (Lada 1992) lie preferentially at the ends of the molecular gas distribution, just as would be predicted by the simplest version of sheet collapse in a noncircular sheet. There are multiple condensations of molecular gas and young stars in these clouds, not just one major cluster at each end of each cloud, but such independent condensations would occur as long as the initial cloud was not a perfectly smooth ellipse.

Dense clusters and dense filamentary gas lie only at one end of the Orion A cloud (e.g., Ali & Depoy 1995; Goldsmith et al. 1997). The other (southern, higher Galactic longitude l) end of the cloud appears to be much more diffuse and contains only small groups of stars (e.g., Strom et al. 1989, 1993). We speculate that this difference is due to initial conditions; the cloud prior to collapse was initially much more diffuse at one end than the other. The overall structure of the A cloud suggests a V shape, with the dense, narrowest region at the northern end (the region of the so-called integral-shaped filament; see Bally et al. 1987). Now, prior to overall collapse to a filament, our calculations for initially elliptical sheets show similar structure at each end; denser concentrations are formed at the “tip” of the ellipse, with two filaments streaming out on either side. We speculate that we are seeing a similar effect in

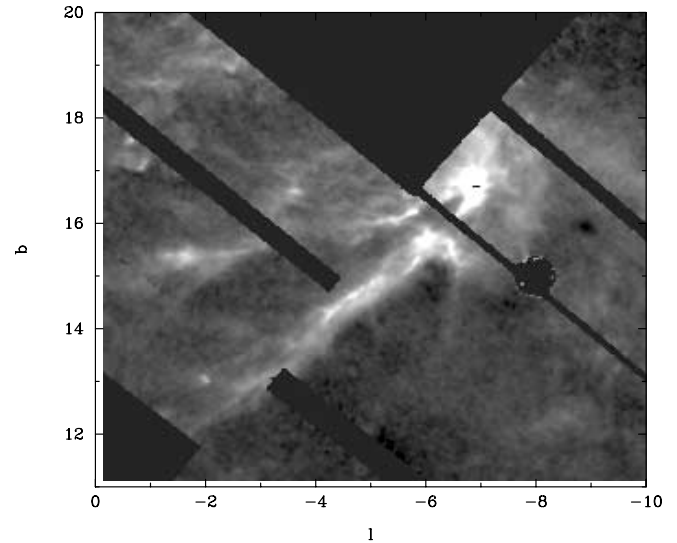


FIG. 14.—Extinction map of the Ophiuchus region made by the COMPLETE project using 2MASS data (Goodman 2004). The major filamentary structures of the cloud and the main concentration of dust (and gas) are evident (see text).

the A cloud; the southernmost parts have not collapsed as far as the northern (lower l) region.

Figure 14³ shows an extinction map of the Ophiuchus region, which more or less indicates the large-scale morphology of the molecular gas. The well-known filamentary structure extending outward from the main concentration of gas and dust is evident. Again, we speculate that the overall structure of this region is due to a collapse similar to that shown at either end of our elliptical sheet calculations, with a “V” of filaments extending out from the main, dense collapse region. The structure is more complex than that of our elliptical sheet simulations, but then the initial conditions are unlikely to be as smooth and simple for real clouds.

Figure 15 shows the distribution of young stars and extinction (which again traces the molecular gas fairly well) in the Cha I cloud. Note how the cloud is filamentary and that once again there are two clear concentrations of stars nearer to the ends of the cloud.

Not all molecular clouds exhibit a simple global filament structure with clusters at the ends. Figure 16 shows the positions of the young stars in the Taurus molecular cloud superposed on the ^{13}CO integrated emission (Mizuno et al. 1995). As noted before (e.g., Hartmann 2002 and references therein), Taurus is composed of extended, roughly parallel bands or filaments of both gas and stars; gravitational fragmentation into several filaments may have occurred (Miyama et al. 1987a, 1987b; Nakajima & Hanawa 1996). There are no major clusters of stars in Taurus (although there is a small double group of stars in L1495; see Fig. 16). Taurus is one of the most dispersed, extended, and low-density clouds, much more extended than regions comparable in mass, such as Ophiuchus. We suggest that the small-scale density and velocity fluctuations inevitably present in any realistic scenario of cloud formation play a much larger role in Taurus than in other regions; the low surface density suggests that global gravitational collapse may not dominate the structure imposed by initial inhomogeneities, in contrast to higher surface density regions.

³ See <http://cfa-www.harvard.edu/COMPLETE>.

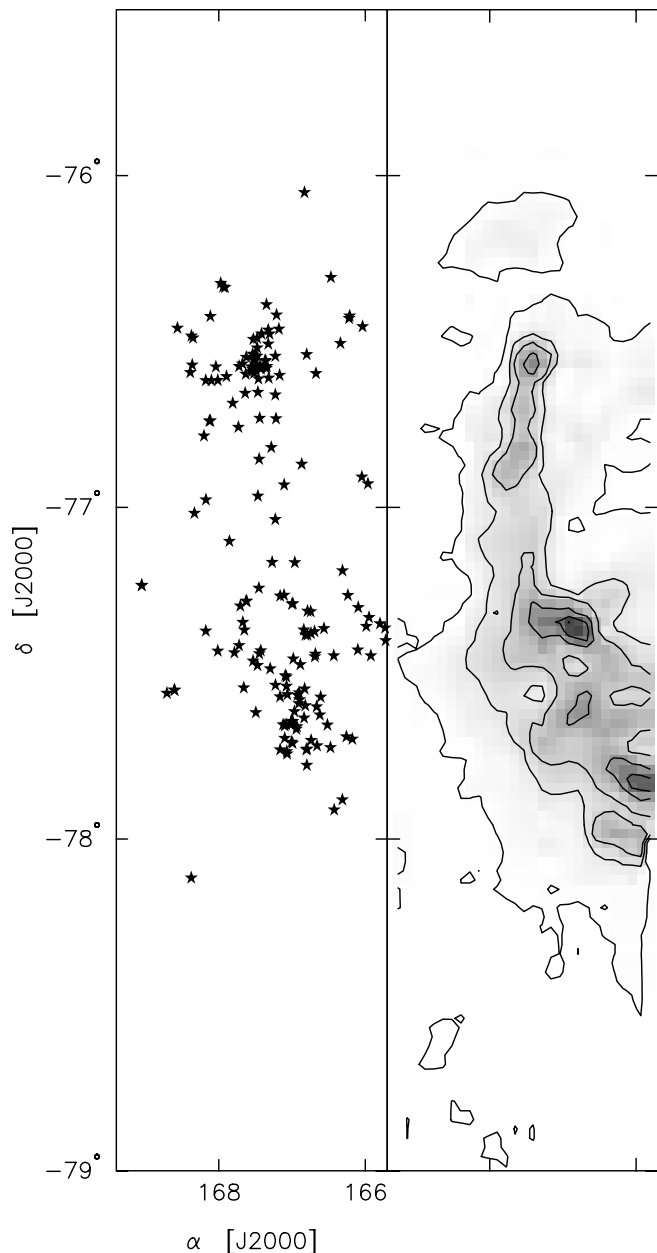


FIG. 15.—Positions of young stellar members (*left*) and extinction contours (*right*) for the Cha I star-forming region, modified from Carpenter et al. (2002) (see text).

However, even in this case of Taurus there is some suggestive substructure. For instance, the double group of L1495 seems to lie at the end of a filament and V-shaped structure running from $l \sim 166^\circ$ to $\sim 169^\circ$; this gas structure seems distinct from other regions, especially as the radial velocities of the gas increase (to positive values) with increasing l , whereas the overall trend in Taurus is increasing radial velocities with decreasing l (e.g., Mizuno et al. 1995). Similarly, there is structure near $l \sim 174^\circ$, $b \sim -13.5^\circ$ (Heiles Cloud 2) that exhibits a curious oval shape with an interior hole as seen in integrated intensity; the young stars also lie along the edge of the oval, suggesting fragmentation in a collapsing cloud edge.

It is worth noting that a number of molecular clouds show a rotation or shear in the line of sight that is comparable to the gravitational acceleration, such as the Orion complex (Bally et al. 1987) and Taurus (e.g., Mizuno et al. 1995). As shown

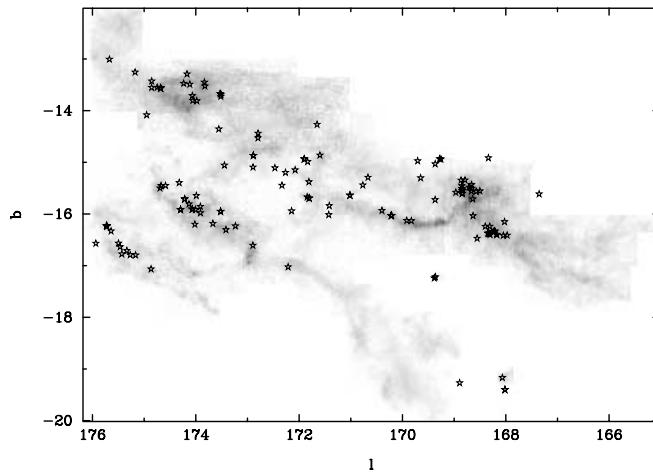


FIG. 16.—Positions of young stars and protostars superposed upon the ^{13}CO integrated emission in Taurus, the latter taken from Mizuno et al. (1995) (see text).

in the simulation of Figure 9, such rotation can slow or prevent the overall collapse of the filament before fragmenting and presumably forming stars. A plausible scenario would be to assume sheets with some angular momentum, insufficient to prevent collapse to a filament but large enough that the resulting filament does not collapse completely. In this kind of picture, there would be a tendency to form filaments with significant rotational support; they would tend to shrink down until arriving at the angular momentum “barrier.”

In summary, we find that several local cloud complexes have morphologies suggestive of the simplest versions of global collapse from a sheetlike configuration; i.e., roughly filamentary cloud structure with concentrations of mass at the end(s) of the clouds.

4.3. Cluster Formation

The simple simulations discussed here may also have particularly important implications for the formation and evolution of star clusters. Many treatments of young clusters assume something like an initial equilibrium configuration and follow the subsequent evolution. However, the simulations presented here suggest that the accumulation of protocluster gas is often a result of gravitational focusing; in other words, that the gas forming the stars is initially collapsing. Formation in collapsing media might result in violent relaxation determining the cluster structure rather than two-body interactions, a result suggested for the very young Orion Nebula cluster by Hillenbrand & Hartmann (1998). Violent relaxation is not restricted to initially highly gravitationally unstable conditions such as a collapsing sheet. In the absence of periodic boundary conditions, initially stabilized but efficiently dissipating turbulent clouds will evolve into global gravitational collapse while fragmenting, with violent relaxation also playing some role in the late phases of evolution (Bate et al. 2003; Bonnell et al. 2003).

In addition, the picture presented here of cluster formation is consistent with the ideas of competitive accretion forming massive stars at the bottoms of cluster gravitational potential wells (Zinnecker 1982; Bonnell et al. 2001a, 2001b). It is worth noting that global infall into focal points can result in the very high local mass infall rates needed to form very massive stars in short times. Alternative pictures in which high infall rates are achieved in static clouds of order one Jeans mass by invoking a high turbulent velocity to support the required high densities

seem implausible. In our picture, global collapse could constitute a substantial fraction of the observed “turbulence” in dense cores, with perhaps smaller scale structure generated by attraction to local mass concentrations.

4.4. Kinematics

A further implication of the simulations is that the “turbulent” motions of many star-forming structures are not necessarily those of a Kolmogorov spectrum but those of gravitationally induced flows with substantially more power on large scales. Another way of saying this is that a substantial component of the observed supersonic line widths in star-forming regions could be the result of collapse rather than small-scale, random turbulent motions. Our simulations are not ideal for exploring this possibility; by restricting the motion to two dimensions and limiting the spatial resolution, we are unable to follow details of the motion. Nevertheless, the idea of global collapse as an important generator of supersonic “turbulence” is very attractive in that some mechanism must be invoked to make gas concentrations in the first place, and star formation must involve gravitationally bound entities.

It is worth noting that, while our nonrotating and non-expanding simulations result ultimately in collapse of all the material to the origin, many real clouds exhibit large-scale velocity gradients along their lengths (e.g., Bally et al. 1987) of a magnitude comparable to that required to prevent total collapse. Such velocity gradients must be the result of initial conditions that generally provide molecular clouds with significant angular momenta.

4.5. Implications for the Initial Mass Function

Our results suggest that there might be some relation between the boundary structure of molecular clouds and the mass distributions of gravitationally focused concentrations, i.e., between cloud edges and stellar/cluster mass functions. Larson (1992) suggested that fractal structure in clouds might be related to the stellar initial mass function; he speculated that the observational indication of fractal projected cloud boundaries (e.g., Falgarone et al. 1991) with fractal dimension $D \sim 1.35$ could be translated into a mass function $dN/d \log M \propto M^{-x}$, with $x \sim 2.35$, consistent with the upper end of the stellar mass function (see also Elmegreen 1997). Our simulations suggest a physical mechanism, gravitational focusing, that can act *directly* on cloud boundaries to form mass concentrations with a distribution that reflects the size distribution of irregularities at

the cloud boundaries. This idea needs further exploration, as subsequent fragmentation and/or competitive accretion could easily modify the mass function resulting simply from edge collapse.

5. CONCLUSIONS

Using numerical simulations of simple, isothermal, finite sheets, we have shown that gravity acting on sheet edges can produce a wide variety of structures that are likely to have some relevance to observed star-forming structures in molecular clouds. In particular, we have shown that a likely general result of the collapse of a sheet formed by flows in the interstellar medium is a filament with higher mass concentrations at the ends of the filament. Any departure from circular symmetry at the edge of gravitationally bound clouds will tend to produce denser concentrations that may be the origin of star clusters. Bastien (1983) found that elongated cylindrical clouds fragmented into two condensations, which he identified as an “end effect” that results from a physical behavior similar to that of collapsing finite sheets. We have shown that several nearby clouds exhibit morphologies that are broadly consistent with the simulations.

We have addressed the problem of finite self-gravitating sheets in as simple a form as possible, limiting the motion to two dimensions. Even with these restrictions, our results emphasize the long-range effects of gravity and the importance of cloud boundaries in generating structure and turbulence. It is likely that clouds are formed with much more structure than assumed here; further steps needed include simulating the formation of molecular clouds from the diffuse interstellar medium to explore what initial density and velocity fluctuations are present. The dynamic nature of even the simple simulations presented here makes it likely that quasi-equilibrium treatments of molecular cloud structure and star formation are unlikely to be realistic. Our initial explorations emphasize the importance of gravitational focusing in creating structure and turbulence in (finite) molecular clouds, a viewpoint that may lead to new observational and theoretical approaches to understanding star formation.

Thanks to John Carpenter for providing a modified version of the Cha I cloud results and to Alyssa Goodman for the extinction map of Ophiuchus. This work was supported in part by NASA grants NAG5-9670 and NAG5-13210.

REFERENCES

- Abramowitz, M., & Stegun, I. A. 1972, *Handbook of Mathematical Functions* (Dover: New York), 591
- Ali, B., & Depoy, D. L. 1995, *AJ*, 109, 709
- Ballesteros-Paredes, J., Vázquez-Semadeni, E., & Scalo, J. 1999, *ApJ*, 515, 286
- Bally, J., Stark, A. A., Wilson, R. W., & Langer, W. D. 1987, *ApJ*, 312, L45
- Bastien, P. 1983, *A&A*, 119, 109
- Bate, M. R., Bonnell, I. A., & Bromm, V. 2002, *MNRAS*, 332, L65
- . 2003, *MNRAS*, 339, 577
- Binney, J., & Tremaine, S. 1987, *Galactic Dynamics* (Princeton: Princeton Univ. Press)
- Bonnell, I. A., & Bastien, P. 1993, *ApJ*, 406, 614
- Bonnell, I. A., Bate, M. R., Clarke, C. J., & Pringle, J. E. 2001a, *MNRAS*, 323, 785
- Bonnell, I. A., Bate, M. R., & Vine, S. G. 2003, *MNRAS*, 343, 413
- Bonnell, I. A., Clarke, C. J., Bate, M. R., & Pringle, J. E. 2001b, *MNRAS*, 324, 573
- Bonnell, I. A., Martel, H., Bastien, P., Arcorogi, J.-P., & Benz, W. 1991, *ApJ*, 377, 553
- Burkert, A., Bate, M. R., & Bodenheimer, P. 1997, *MNRAS*, 289, 497
- Burkert, A., & Bodenheimer, P. 1993, *MNRAS*, 264, 798
- Burkert, A., & Bodenheimer, P. 1996, *MNRAS*, 280, 1190
- Carpenter, J. M., Hillenbrand, L. A., Skrutskie, M. F., & Meyer, M. R. 2002, *AJ*, 124, 1001
- Colella, P., & Woodward, P. 1984, *J. Comput. Phys.* 54, 174
- de Avillez, M. A., & Mac Low, M. 2001, *ApJ*, 551, L57
- Elmegreen, B. G. 1997, *ApJ*, 486, 944
- . 2000, *ApJ*, 530, 277
- . 2002, *ApJ*, 577, 206
- Falgarone, E., Phillips, T. G., & Walker, C. K. 1991, *ApJ*, 378, 186
- Gammie, C. F., Lin, Y., Stone, J. M., & Ostriker, E. C. 2003, *ApJ*, 592, 203
- Goldsmith, P. F., Bergin, E. A., & Lis, D. C. 1997, *ApJ*, 491, 615
- Goodman, A. 2004, in *ASP Conf. Ser. 323, Star Formation in the Interstellar Medium*, ed. D. Johnstone et al. (San Francisco: ASP), in press
- Hartmann, L. 2002, *ApJ*, 578, 914
- Hartmann, L., Ballesteros-Paredes, J., & Bergin, E. A. 2001, *ApJ*, 562, 852 (HBB01)
- Hillenbrand, L. A. 1997, *AJ*, 113, 1733
- Hillenbrand, L. A., & Hartmann, L. W. 1998, *ApJ*, 492, 540
- Hunter, C. 1963, *MNRAS*, 126, 299
- Klessen, R. S., & Burkert, A. 2000, *ApJS*, 128, 287

- Klessen, R. S., & Burkert, A. 2001, *ApJ*, 549, 386
Klessen, R. S., Heitsch, F., & Mac Low, M. 2000, *ApJ*, 535, 887
Lada, E. A. 1992, *ApJ*, 393, L25
Larson, R. B. 1985, *MNRAS*, 214, 379
———. 1992, *MNRAS*, 256, 641
Li, P. S., Norman, M. L., Mac Low, M., & Heitsch, F. 2004, *ApJ*, 605, 800
Mac Low, M.-M., Klessen, R. S., Burkert, A., & Smith, M. D. 1998, *Phys. Rev. Lett.*, 80, 2754
Mestel, L. 1963, *MNRAS*, 126, 553
Miyama, S. M., Narita, S., & Hayashi, C. 1987a, *Prog. Theor. Phys.*, 78, 1051
———. 1987b, *Prog. Theor. Phys.*, 78, 1273
Mizuno, A., Onishi, T., Yonekura, Y., Nagahama, T., Ogawa, H., & Fukui, Y. 1995, *ApJ*, 445, L161
Monaghan, J. J. 1994, *ApJ*, 420, 692
Nakajima, Y., & Hanawa, T. 1996, *ApJ*, 467, 321
Nelson, R. P., & Papaloizou, C. B. 1993, *MNRAS*, 265, 905
Ostriker, E. C., Gammie, C. F., & Stone, J. M. 1999, *ApJ*, 513, 259
Padoan, P., & Nordlund, Å. 1999, *ApJ*, 526, 279
Passot, T., Vazquez-Semadeni, E., & Pouquet, A. 1995, *ApJ*, 455, 536
Schneider, S., & Elmegreen, B. G. 1979, *ApJS*, 41, 87
Strom, K. M., Margulis, M., & Strom, S. E. 1989, *ApJ*, 346, L33
Strom, K. M., Strom, S. E., & Merrill, K. M. 1993, *ApJ*, 412, 233
Tohline, J. E. 1980, *ApJ*, 239, 417
Truelove, J. K., Klein, R. I., McKee, C. F., Holliman, J. H., Howell, L. H., & Greenough, J. A. 1997, *ApJ*, 489, L179
Vazquez-Semadeni, E., Passot, T., & Pouquet, A. 1995, *ApJ*, 441, 702
Wada, K., & Norman, C. A. 2001, *ApJ*, 547, 172
Wilson, A. 2001, Ph.D. thesis, Harvard Univ.
Wyse, A. B., & Mayall, N. U. 1942, *ApJ*, 95, 24
Zinnecker, H. 1982, in *Ann. NY Acad. Sci.*, 395, Symposium on the Orion Nebula to Honor Henry Draper, ed. A. E. Glassfold et al., 226